Universiteit
Antwerpen

This item is the archived peer-reviewed author-version of:

Numerical investigation of HBr/He transformer coupled plasmas used for silicon etching

Reference:
Gul Banat, Tinck Stefan, De Schepper Peter, Aman-ur-Rehman, Bogaerts Annemie.- *Numerical investigation of HBr/He transformer coupled plasmas used for silicon etching*
Journal of physics: D: applied physics - ISSN 0022-3727 - 48:2(2015), p. 1-9
DOI: http://dx.doi.org/doi:10.1088/0022-3727/48/2/025202

uantwerpen.be
Institutional repository IRUA

Numerical Investigation of HBr/He Transformer Coupled Plasmas used for Silicon Etching

Banat Gul[1, 2], Stefan Tinck[1] , Peter De Schepper[3], Aman-ur-Rehman[2] , Annemie Bogaerts[1]
[12]*Research Group PLASMANT, Department of Chemistry, University of Antwerp, Universiteitsplein 1 B-2610, Antwerp, Belgium*
[21]*Department of Physics and Applied Mathematics, Pakistan Institute of Engineering and Applied Sciences, Nilore, Islamabad 45650, Pakistan.*
[3]Interuniversity Microelectronics Centre, Kapeldreef 75 B-3001, Leuven, Belgium

E-mai: amansadiq@gmail.com

Abstract

A two-dimensional hybrid Monte Carlo - fluid model is applied to study HBr/He inductively coupled plasmas used for etching of Si. Complete sets of gas-phase and surface reactions are presented and the effects of the gas mixing ratio on the plasma characteristics and on the etch rates are discussed. A comparison with experimentally measured etch rates is made to validate the modelling results. The etch rate in the HBr plasma is found to be quite low under the investigated conditions compared to typical etch rates of Si with F- or Cl-containing gases. This allows for a higher control and fine-tuning of the etch rate when creating ultra-small features. Our calculations predict a higher electron temperature at higher He fraction, because the electrons do not lose their energy so efficiently in vibrational and rotational excitations. As a consequence, electron impact ionization and dissociation become more important, yielding higher densities of the ions, the electrons and H atoms. This results in more pronounced sputtering of the surface. Nevertheless, the overall etch rate decreases upon increasing He fraction, suggesting that chemical etching is still the determining factor for the overall etch rate.

Introduction

Plasma etching is one of the many basic steps for the fabrication of electronic devices used in semiconductor processing. In the semiconductor industry, halide containing plasmas, such as fluorine, chlorine, and bromine are typically used for etching of silicon [1, 2]. For most patterned etching processes, it is desirable to have anisotropic, selective and uniform etching. However, it is difficult to achieve all these goals simultaneously, and unwanted etching artifacts like undercutting, notching, bowing, micro-trenching are often observed. A proper control of the etch rate is therefore indispensable.

Popular halides to etch Si are fluorine, chlorine and bromine, because they form volatile products during etching (i.e., SiF_4, $SiCl_4$ or $SiBr_4$). Fluorine is very popular because of its high etch rate of Si. Indeed, of all halides, fluorine is the most reactive towards a silicon surface. Unfortunately, fast chemical reactions of F atoms often lead to undercutting of the mask, resulting in loss of anisotropy [3, 4]. To maintain anisotropy, plasma etching is typically a combination of ion and radical bombardment, i.e., ion assisted etching rather than pure chemical etching [5]. For example, in the absence of ion bombardment, Si is etched very slowly by Cl [3, 6, 7], but fairly high etch rates and anisotropic profiles can be obtained with ion-assisted etching using chlorine plasmas. Chlorine-based plasmas, however, also occasionally present some problems. Indeed, the etch profiles often deviate from ideal vertical sidewalls and the selectivity with respect to etching of SiO_2 or photoresist masks is often not as high as desired.

In comparison to chlorine- and fluorine-based plasmas, bromine plasmas have superior anisotropy and selectivity for etching of single crystal and poly-crystalline Si, as well as higher selectivity towards SiO_2,

Si_3N_4, and organic photoresists [8-10]. Bromine is less reactive towards silicon than chlorine, and room-temperature chemical etching with bromine does not occur spontaneously. The purely chemical etch rate of Si with bromine is therefore much lower (i.e., negligible) and therefore sufficient ion bombardment is needed. Ion sputtering enhances the actual etching by providing the activation energy for desorption of the volatile etch product (i.e. $SiBr_4$), which does not necessarily need a high ion energy. Especially for the latest developments in electronic device fabrication, where features are extremely small, low etch rates are often preferred to create very thin layers or extremely small nanostructures. In spite of the lower etch rate compared to F and Cl plasmas, Br plasmas thus can provide a more controlled etch process and can produce more anisotropic feature profiles and higher selectivity during etching [11-13]. A few years ago, fluorine or chlorine, usually in combination with oxygen, were sufficient to control sidewall etching of silicon for fabricating devices of the desired size, but as features keep shrinking, increasingly complex gas mixtures, containing CF_4, CHF_3, SF_6 and HBr, become more and more popular to make the ultra-small electronic devices.

Today, in microelectronics, HBr is often used for plasma etching in various mixtures, for example combined with Ar, F_2, Br_2, Cl_2, SF_6/O_2, BCl_3, CH_4, H_2, He or even as a pure gas [14-23]. However, even relatively simple binary systems, like mixtures of HBr with Ar or He, are not yet fully understood, because of the poor knowledge of the physicochemical processes and because HBr was not so popular a few years ago for etching Si, when F_2 and Cl_2 still provided enough etch control.

Numerical modelling is an attractive way to analyse the plasma physics and chemistry in these low pressure and low temperature industrial plasmas. A number of papers have been published on the modelling of bromine-based plasmas, like HBr/Ar, HBr/Cl_2, and HBr/He [14-18]. All these papers, however, use zero-dimensional models to investigate the bulk plasma characteristics and thus they provide no information on the shape and uniformity of the plasma and on how the species behave near the reactor walls and the wafer. In the present work, we apply a two-dimensional model to investigate different HBr/He gas mixtures to illustrate how the addition of a noble gas influences the plasma characteristics like the species -density profile in the reactor volume as well as the etch rate along the complete surface of the wafer. The model will be compared with experimentally obtained etch rates for validation.

Description of the model

The so-called hybrid plasma equipment model (HPEM), developed by Kushner and co-workers, is applied to describe the plasma processes [24]. HPEM treats the fast electrons in a Monte Carlo module and the heavy plasma species in a fluid module. HPEM has three main modules: the electromagnetics module (EMM), the electron energy transport module (EETM) and the fluid kinetics module (FKM). The EMM calculates the electrostatic and electromagnetic fields within the reactor by solving Maxwell's equations. These fields are transferred to the EETM, which can use either a Monte Carlo approach or a Boltzmann solver to obtain the electron impact source functions and the electron transport coefficients. The results from the EETM are then transferred to the FKM to compute the densities, fluxes, and temperatures of all plasma species and to solve Poisson's equation for the electrostatic potential. The FKM output is fed back to the EMM for an updated calculation of the electromagnetic fields. The HPEM iterates through these three coupled modules to calculate the plasma characteristics until a converged and stable solution is reached.

1 In addition to this plasma model, an extra analytical model is applied to calculate changes in the
2 composition of the surface layers due to etching, sputtering or deposition by plasma species. This allows
3 us to calculate the etch rates and the chemical composition of the surface during etching under well-
4 defined conditions. From this analytical model, the fluxes of surface species returning to the plasma, like
5 the etch products, are defined for an updated calculation of the plasma behavior.

6 In the following sections, the reaction sets for the bulk plasma and surface chemistry of a HBr/He plasma
7 are presented and discussed.

8 *2.1. Species considered in the model*

9 In total, 17 different plasma species are taken into account. In addition, 10 different surface species are
10 included for addressing the plasma-surface interactions of the HBr/He plasma with the Si wafer. The
11 complete list of species is presented in **table 1**.

12 **Table 1**. Overview of the species included in the model.

Ground state neutrals:	He, HBr, Br, Br_2, H, H_2
Positive ions:	He^+, HBr^+, Br^+, Br_2^+, H^+, H_2^+, H_3^+
Excited species:	He*, Br*
Negatively charged species:	Br^-, electrons
Surface species:	$Si_{(s)}$, $SiH_{(s)}$, $SiH_{2(s)}$, $SiH_{3(s)}$, $SiBr_{(s)}$, $SiBr_{2(s)}$, $SiBr_{3(s)}$, $SiHBr_{(s)}$, $SiHBr_{2(s)}$, $SiH_2Br_{(s)}$

13

14 He* and Br* are the electronically excited He and Br atoms. He* has an energy level of 19.8 eV while the
15 Br* species comprises the 4*s*, 4*p*, 3*d*, 5*p*, 4*d*, and 5*d* electronic excitation levels with energies of 8.9 eV,
16 10.4 eV, 10.9 eV, 11.8 eV, 12.0 eV and 12.4 eV, respectively. The excited levels of H_2 are not explicitly
17 incorporated in the model, but they are included in the H_2 species, i.e., the latter consists of the ground
18 state, two electronic excited levels, with threshold of 8.8 eV and 11.87 eV, as well as two rotational and
19 two vibrational levels, with threshold energies of 0.04 eV, 0.07 eV, 0.52 eV and 1.0 eV, respectively.
20 Similarly, for HBr, three vibrational states are included, with energy levels of 0.3 eV, 0.6 eV and 0.9 eV
21 [24].

22 As for the etch products, various SiH_xBr_y species ($x \geq 0$, $y \geq 0$, $x+y \leq 4$) can occur in the bulk plasma.
23 However, insufficient data is available to properly model the SiH_xBr_y products, so electron impact
24 reactions of these species are not considered in the model. This is justified as these etch products have
25 very low densities in the plasma, because the etch rate is very low, as will be shown in the results section,
26 so it is impossible for the etch products to accumulate in the plasma before they are pumped out.
27 However, several SiH_xBr_y($x \geq 0$, $y \geq 0$, $x+y \leq 4$) species are considered in the surface reaction set to calculate
28 the chemical composition of the surface during etching.

29 *2.2 Plasma chemical reactions included in the model*

30 To describe the plasma chemistry of the HBr/He plasma, a detailed reaction set was constructed which is
31 presented in **tables 2** and **3**. The electron-impact collisions are shown in **table 2.** The rates of these
32 reactions are defined by energy-dependent cross sections $\sigma(E)$ that can be found in the corresponding

1 references. The rates of the ion–ion, ion–neutral and neutral–neutral reactions are determined by reaction
2 rate coefficients that are directly presented in **table 3**. Elastic collisions between electrons and the other
3 heavy plasma species are included in the model but not listed in the tables. The total plasma reaction set,
4 including the elastic collisions, consists of 73 gas phase reactions. Note that in **table 3** several "general"
5 reactions are indicated, which stand for several individual reactions occurring with different species
6 (denoted by X and Y).

7 **Table 2**. Overview of the inelastic electron impact reactions included in the model, with the references where the cross sections are adopted from.
8 E_{th} is the threshold energy for the reaction.

Reaction	Reaction type	E_{th} (eV)	Reference
$e + He \rightarrow He^* + e$	Electronic excitation	19.80	[25]
$e + He \rightarrow He^+ + e$	Ionization	24.54	[25]
$e + He^* \rightarrow He^+ + 2e$	Ionization	4.73	[25]
$e + He^* \rightarrow He + e$	De-excitation	0	[25]
$e + H_2 \rightarrow H + H + e$	Dissociation	8.8	[26]
$e + H_2 \rightarrow H_2^+ + 2e$	Ionization	15.43	[27]
$e + H_2^+ \rightarrow H + H$	Dissociative recombination	0.00	[28]
$e + H \rightarrow H^+ + 2e$	Ionization	13.56	[29]
$e + H_3^+ \rightarrow H^+ + H_2 + e$	Dissociation	14.9	[28]
$e + H_3^+ \rightarrow H + H_2$	Dissociative recombination	0.00	[28]
$e + HBr \rightarrow Br + H + e$	Dissociation	6.6	[24]
$e + HBr^+ \rightarrow Br + H$	Dissociative recombination	0.00	[24]
$e + HBr \rightarrow Br^- + H$	Dissociative attachment	0.08	[24]
$e + HBr \rightarrow HBr^+ + 2e$	Ionization	12.74	[24]
$e + Br \rightarrow Br^* + e$	Electronic excitation	see text	[24]
$e + Br \rightarrow Br^+ + 2e$	Ionization	12.99	[24]
$e + Br^- \rightarrow Br + 2e$	Neutralization	3.61	[24]

9

10

11 **Table 3.** Overview of the heavy particle reactions included in the model, with the rate coefficients and corresponding
12 references. X = HBr, Br, Br_2, H, H_2, H_3 or He, and Y = HBr, Br or Br_2. * denotes reactions whose rate coefficients were
13 estimated, due to lack of data in literature. These are charge transfer reactions which typically have a rate constant in the
14 order of 10^{-10} - 10^{-11} cm^3 s^{-1}.

Reaction	Rate constant (cm^3 s^{-1})	Reference
$H + HBr \rightarrow H_2 + Br$	6.5×10^{-12}	[14]
$H + Br_2 \rightarrow HBr + Br$	7.3×10^{-11}	[14]

$Br^- + X^+ \rightarrow Br + X$	1.0×10^{-7}	[15]
$He^* + HBr \rightarrow H + Br + He$	5.0×10^{-12}	[15]
$He^* + H_2 \rightarrow H + H + He$	5.0×10^{-12}	[15]
$H_2^+ + H \rightarrow H_2 + H^+$	6.4×10^{-10}	[30]
$H_2^+ + H_2 \rightarrow H_3^+ + H$	2.0×10^{-9} [T / 298 K]$^{-0.5}$	[31]
$H_2^+ + Y \rightarrow H_2 + Y^+$	1.0×10^{-11}	*
$H^+ + Y \rightarrow H + Y^+$	1.0×10^{-11}	*
$He^+ + Y \rightarrow He + Y^+$	1.0×10^{-11}	*
$He^+ + H \rightarrow He + H^+$	1.0×10^{-11}	*
$He^+ + H_2 \rightarrow He + H_2^+$	1.0×10^{-11}	*
$Br^+ + HBr \rightarrow Br + HBr^+$	1.0×10^{-11}	*
$Br^+ + Br_2 \rightarrow Br + Br_2^+$	1.0×10^{-11}	*
$HBr^+ + Br_2 \rightarrow HBr + Br_2^+$	1.0×10^{-11}	*
$He^* + He^* \rightarrow He^+ + He + e$	1.6×10^{-9}	[25]

1

2 *2.3 Surface reactions included in the model*

3 In total 128 surface reactions are considered in the model, including both chemical reactions of neutrals
4 and sputtering by ions (see below). **Table 4** shows the reaction probabilities for the interactions of the
5 different neutral plasma species with the various surface layers. Reaction probabilities for bromine with
6 silicon are not so well known; therefore, a similar mechanism was followed as in [32], where Si is etched
7 with Cl and F. Indeed, in principle the same reactions happen when halides like F, Cl or Br etch silicon,
8 but with different probabilities, since F is more reactive than Cl, which is in turn more reactive than Br.
9 Based on this knowledge, we have estimated surface reaction probabilities for Br on Si, following the
10 same reaction mechanism as presented by Hoekstra et al. [32], and based on comparing the calculated
11 etch rates with measured values. We will show in section 3.3 below that the calculated etch rates are
12 indeed in good agreement with the measured values, which indicates that the surface reaction
13 probabilities assumed here, are reasonable.

14

15 **Table 4**. Overview of the surface processes of the neutral species, taken into account in the model.

Surface reaction	Probability	Reference
$Br + SiBr_{x(s)} \rightarrow SiBr_{x+1(s)}$ (x = 0 - 3)	1.00, 0.10, 0.10, 0.01	[32]
$Br + SiH_{x(s)} \rightarrow SiH_xBr_{(s)}$ (x = 1 - 3)	0.10, 0.10, 0.01	[32]
$Br + SiH_{x(s)} \rightarrow SiH_{x-1(s)} + HBr$ (x = 1 - 3)	0.20, 0.20, 0.20	[34]
$Br + SiHBr_{x(s)} \rightarrow SiHBr_{x+1(s)}$ (x = 1 - 2)	0.10, 0.01	[32]

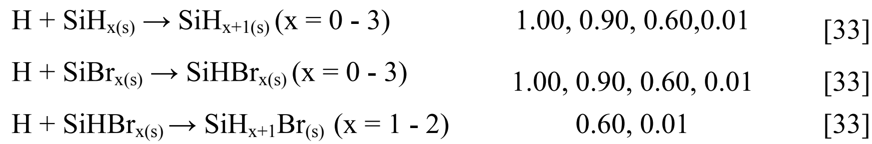

$H + SiH_{x(s)} \rightarrow SiH_{x+1(s)}$ (x = 0 - 3)	1.00, 0.90, 0.60,0.01	[33]
$H + SiBr_{x(s)} \rightarrow SiHBr_{x(s)}$ (x = 0 - 3)	1.00, 0.90, 0.60, 0.01	[33]
$H + SiHBr_{x(s)} \rightarrow SiH_{x+1}Br_{(s)}$ (x = 1 - 2)	0.60, 0.01	[33]

The surface reactions presented in **table 4** describe the chemical etching of silicon with bromine and hydrogen. The sticking probability for neutrals on the surface is taken to be 1 for both reactants Br and H on clean Si. Even though H will react more eagerly than Br overall, their sticking probabilities are both 100% on clean Si since this type of surface has a high density of dangling bonds so that H and Br both will practically always stick. Br and H atoms will bind with Si surface atoms to form a SiH_xBr_y ($x + y < 4$) layer. The more Br atoms bonded to a Si surface atom, the weaker the $SiBr_x$ molecule is bound to the surface. Eventually the Si atom can be extracted from the surface in the form of $SiBr_4$, SiH_4 or any possible combination of SiH_xBr_y ($x + y = 4$), which are volatile molecules. However, the spontaneous chemical etching of Si in the form of $SiBr_4$ without ion bombardment is very slow and practically negligible. This is due to the fact that when $SiBr_4$ is formed, it will remain stuck to the surface before it can thermodynamically desorb. The actual desorption of $SiBr_4$ will be assisted by ion bombardment or by heating of the surface [35]. Compared to Br atoms, Br_2 molecules are less reactive towards a silicon surface because Br_2 is a stable molecule and less eager to chemically react with silicon. The same is true for HBr. It is also worth mentioning that the etch products containing both bromine and hydrogen atoms, SiH_xBr_y($x\geq0$, $y\geq0$, $x+y=4$), can be more volatile than $SiBr_4$ itself [36].

Beside the neutral species, the ions can also bombard the surface, and they will give rise to sputtering. This can be represented by one general equation:

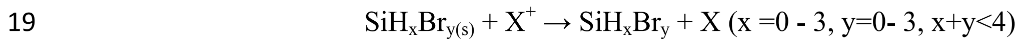

$$SiH_xBr_{y(s)} + X^+ \rightarrow SiH_xBr_y + X \quad (x = 0 - 3,\ y = 0 - 3,\ x+y<4)$$

Where X^+ stands for He^+, Br^+, Br_2^+ or HBr^+. Hence, this equation illustrates the surface reactions that can occur for the He^+, Br^+, Br_2^+ or HBr^+ ions. Sputtering by H^+, H_2^+ or H_3^+ ions is not included, because it is negligible due to the small mass of these ions, i.e., the energy transfer is very poor to create a significant collision cascade. The same is in principle true for He^+ ions, but as they are more abundant in the plasma, certainly at high He fractions in the gas mixture, sputtering by He^+ ions is explicitly included.

The sputter yields for He^+, Br^+, and Br_2^+ ions implemented in our model, are plotted as a function of bombarding energy in **figure 1**, both on pure poly-Si (a), and on various SiH_xBr_y surface (b). The sputter yields on poly-Si are based on the so called Matsunami formula [37]. Indeed, Matsunami et al. [37] proposed a formula based on experimental data to predict the sputter yield of various monoatomic ions on various surfaces. Although the formula is in principle only valid for monoatomic ions, due to the small mass difference between HBr and Br, the sputter yield of HBr^+ was considered to be the same as that of Br^+(therefore, the sputter yield of HBr^+ ions is not explicitly shown in figure 1). Moreover, the sputter yield of Br_2^+ is defined as twice the sputter yield of Br^+ but at half of the kinetic energy, because the energy of the of Br_2^+ ion has to be split over its fractions i.e, as Br atom and a Br^+ ion. These sputter yields are valid for ions arriving perpendicular to the surface, which is true here for practically all ions, as they are accelerated through the sheath.

The Br and H neutral fluxes to the wafer will significantly increase the sputter yield due to chemical transformation of Si to SiH_xBr_y which is more easily sputtered. We could not find sufficient data for the sputter yields of SiH_xBr_y layers; therefore, we assumed values based on yields proposed by Hoekstra et al. [32] for sputtering of $SiCl_x$ layers under similar operating conditions. This is based on the principle that, the less bonds the Si atom (in the form of SiHxBry) has with the Si-bulk, the more easily it can be detached from the surface by ion bombardment, which is logical.

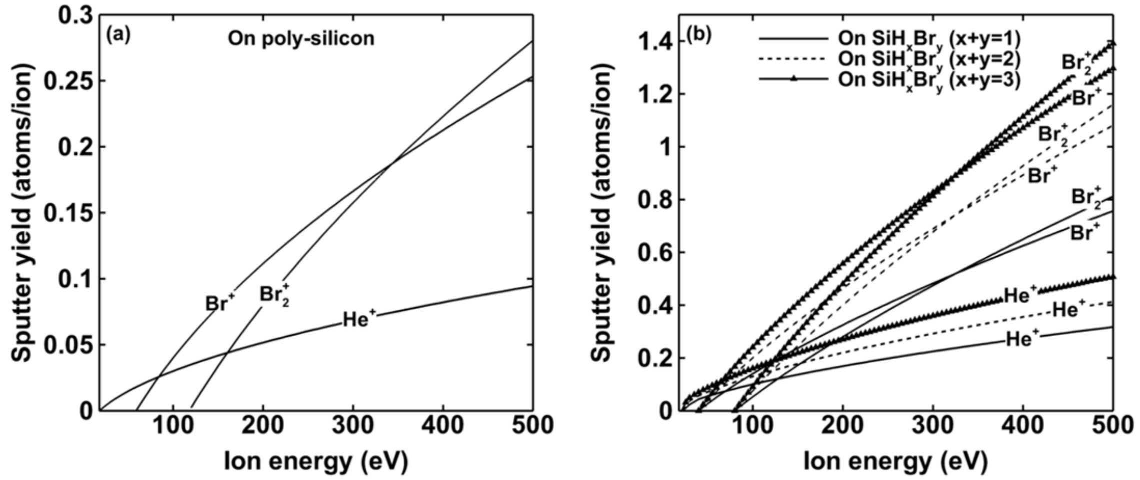

Figure 1. Sputter yields of He^+, Br^+, Br_2^+ , as a function of ion energy, for perpendicular ion bombardment, as implemented in the model, on poly-Si (a) and on the various SiH_xBr_y layers (b) . The sputter yields of H^+, H_2^+ and H_3^+ are negligible due to their low mass. The sputter yield of HBr^+ is considered to be the same as that of Br^+ (see text).

Results and discussion

3.1. General plasma characteristics

Calculations were performed for HBr/He mixtures in a transformer coupled plasma reactor (TCP) of which the geometry is shown in **figure 2,** under the following operating conditions: 60 mTorr total gas pressure, 450 sccm total gas flow rate for a mixture of 20% He and 80% HBr, 800 W source power, -223 V dc bias at the substrate electrode and an operating frequency of 13.56 MHz applied to the coil and to the substrate electrode. The defined -223 V bias voltage corresponds here to a bias power of 76W.

1

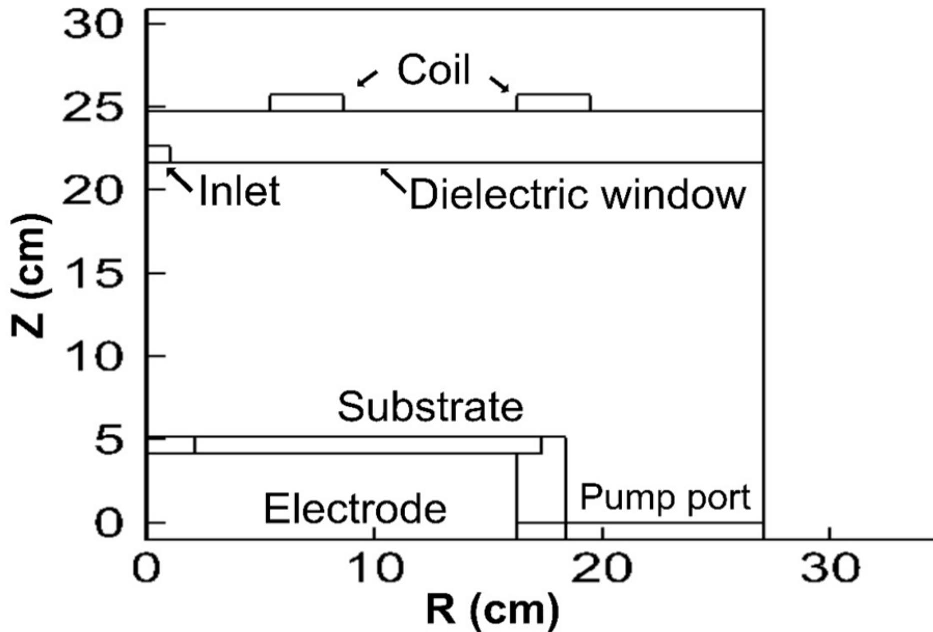

2 **Figure 2.** Two-dimensional TCP reactor geometry defined in the model. The reactor is cylindrically symmetric, so only a half
3 plane of the reactor is shown. By rotating the plane around the left axis, the full reactor volume is obtained.

4 **Figure 3** shows the calculated density profiles of different plasma species in the reactor volume, averaged
5 over one rf cycle. The background gases (HBr and He) and the Br radicals have the highest densities in
6 the reactor. HBr and He have a maximum density near the inlet as expected, and their densities show a
7 minimum in the area where the plasma density is the highest, i.e., directly underneath the coil, where most
8 electron impact reactions occur, due to the higher electron temperature (see below). Wall recombination
9 and neutralization reactions of the other plasma species again raise the densities of HBr and He near the
10 walls. It is clear from figure 3 that under these conditions, the HBr background gas is highly dissociated.
11 Indeed, the HBr density in the bulk plasma is one order of magnitude lower than the density at the inlet,
12 and the density of the Br atoms in the bulk plasma even exceeds that of HBr. The drop in HBr density is
13 far more pronounced than for He, where the difference between the bulk density and the inlet density is
14 only a factor of 2. This is logical, because He can only be ionized or excited, which requires a higher
15 threshold energy (see table 2). Besides HBr, He and Br, also the H atoms have a non-negligible density in
16 the plasma, with a maximum underneath the coil, where most electron impact dissociation takes place.

17 The most important ions present in the bulk plasma are HBr^+, Br^+ and Br^-. The other ions have
18 significantly lower densities and are therefore not shown. Indeed, HBr and Br are the most abundant
19 neutral species, so it is logical that their corresponding ions are most important. The He^+ ions are not so
20 abundant because of the 20% He gas fraction, and because of the high ionization threshold (i.e., 24.59
21 eV). The ionization thresholds for HBr and Br are only 12.74 eV and 12.99 eV, respectively, which is
22 significantly lower, thus the HBr^+ and Br^+ are formed more easily than He^+. Furthermore, these values are
23 also slightly lower than the ionization threshold of H atoms (13.56 eV). As a result, the charge transfer
24 reaction between H^+ ions and HBr or Br, creating HBr^+ or Br^+ with H, is favoured in this direction.
25 Finally, Br^- is formed by electron impact dissociative attachement of HBr, which has a threshold energy
26 of 0.08 eV.

1 The maximum Br^+ density (~$9x10^{11}$ cm^{-3}) is still about one order of magnitude higher than the maximum
2 HBr^+ density (~$9x10^{10}$ cm^{-3}), which follows the behaviour of the corresponding neutrals. The ionization
3 degree of Br and HBr is in order of 10^{-3} -10^{-4}. The maximum Br^- density is ~ $3.4x10^{11}$ cm^{-3}, while the
4 maximum electron density is ~ $5.5x10^{11}$ cm^{-3}, as is clear from figure 3. These Br^+, Br^- and electron
5 densities all have their maximum underneath the coil, where the power deposition is highest, as expected.
6 The HBr^+ density, on the other hand, shows a maximum in the center of the reactor, because its precursor
7 (HBr) also has a maximum density in this area (near the nozzle).

8 The gas temperature in the plasma has a torus-shaped maximum of about 850 K, following the windings
9 of the coil, as shown in **figure 4(a)**. Indeed, the electromagnetic fields generated by the coil are strongest
10 here, resulting in a higher acceleration of the electrons and also more gas heating. In the center of the
11 reactor, the gas is colder due to the centrally located nozzle, which injects the room-temperature HBr/He
12 feed gas. The electron temperature, averaged over 1 rf cycle, reaches a maximum of about 2.8 eV
13 underneath the coil, as expected (see **figure 4b**).

14

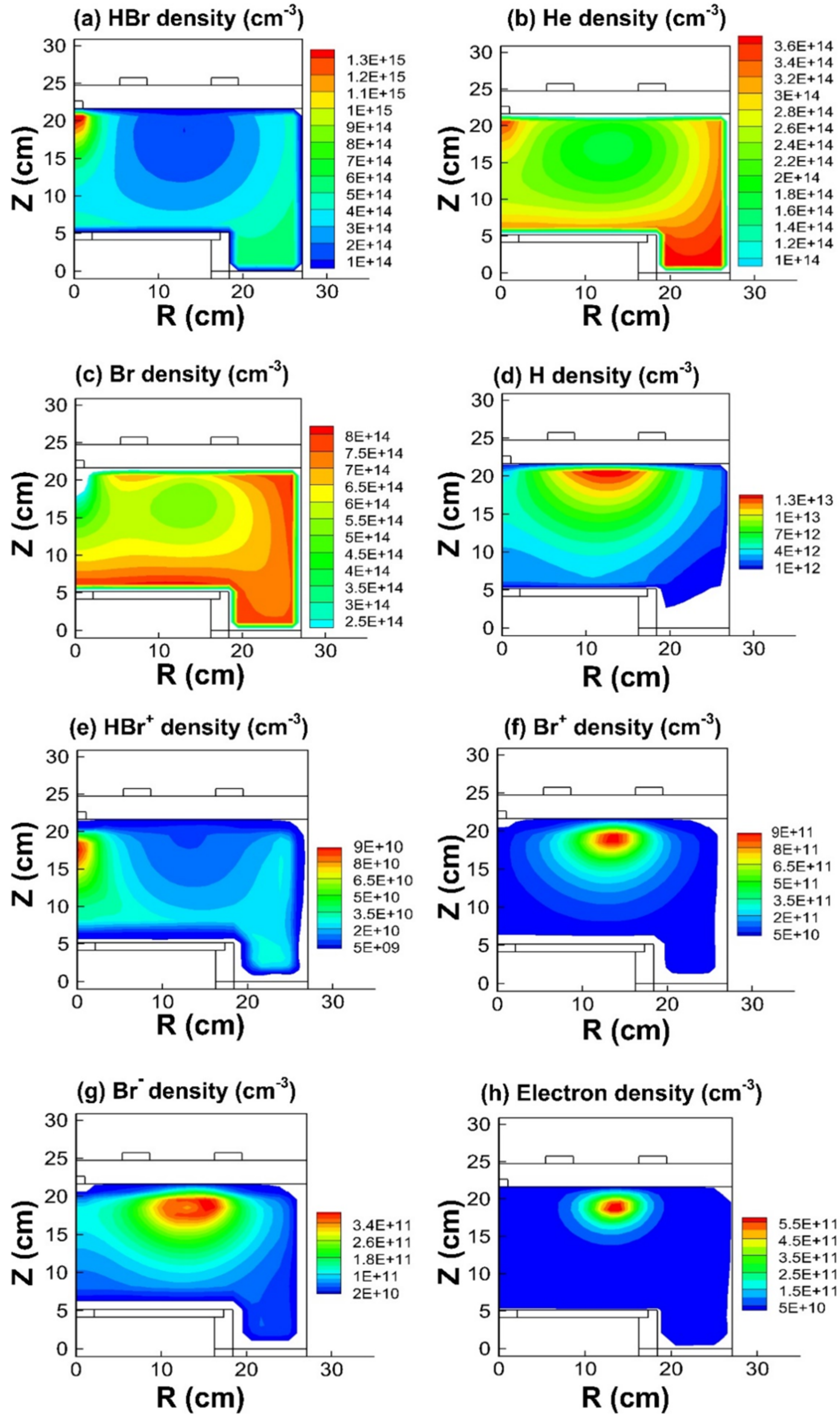

1

1 **Figure 3.** Calculated density profiles of the most important neutrals and ions, for a 20% He and 80% HBr gas mixture. The
2 operating conditions are: 60 mTorr total gas pressure, 450 sccm gas flow rate, 800 W source power, -223 dc bias at the substrate
3 and 13.56 MHz operating frequency at the coil and at the substrate electrode.

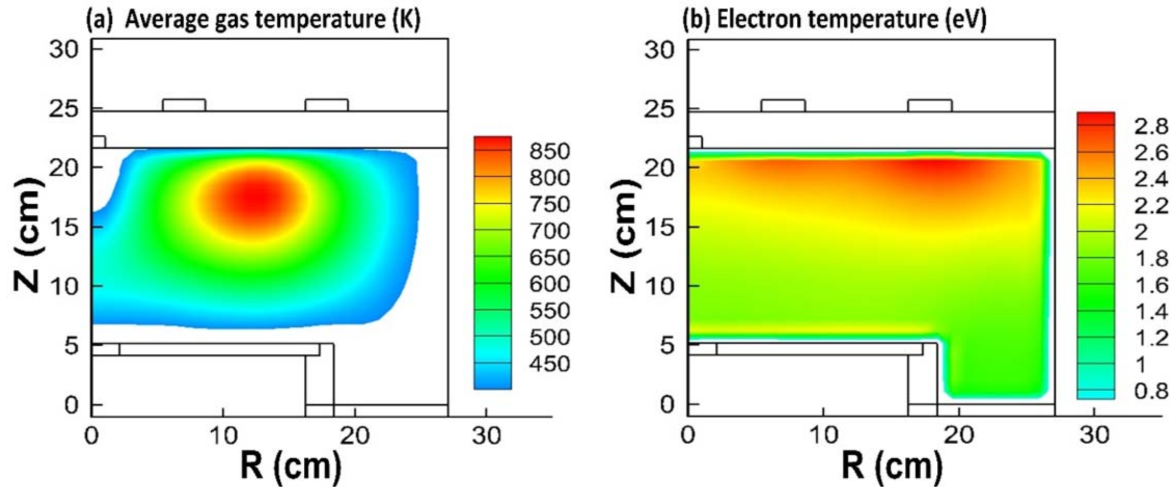

4

5 **Figure 4.** Calculated gas (a) and electron (b) temperature profiles for the same operating conditions as in figure 3.

6 *3.2. Influences of the gas mixture on the plasma properties*

7 **Figure 5** shows the volume averaged densities of the most relevant neutrals and ions for etching, as a
8 function of the He fraction in the HBr/He mixture. The densities of HBr and Br decrease upon increasing
9 He fraction, which is logical. However, the HBr density decreases more than linearly, whereas the drop in
10 the Br density is less pronounced. This suggests that the dissociation degree of HBr is larger when there is
11 more He in the plasma. Indeed, the overall gas mixture then becomes more atomic, and rotational and
12 vibrational excitations occur less often, so the electron energy loss in the low and medium part of the
13 EEDF is reduced. Moreover, the electron impact reactions with He have higher threshold energies (see
14 **table 2**) and will not occur so often. This results in an increase of the electron temperature with rising He
15 fraction, as illustrated in **figure 6**, allowing the electrons to perform more ionizations and dissociations.
16 This increase in the electron temperature upon rising He fraction is in good correlation with the Langmuir
17 probe diagnostics reported by Ham et al. [16] and the same effect was also observed by Cheng et al. [11].
18 In addition, the bias power changes gradually from 70W at 0% He to 145W at 100% He. This is
19 because at higher He fraction, the total ion density becomes higher so the electric field generated
20 by the substrate bias is more strongly quenched by the higher ion density. Therefore, to create the
21 -223 V volt, more bias power is needed.

22 The more pronounced dissociation of HBr at higher He gas fractions also explains the rise in H density
23 upon rising He fraction, in spite of the lower HBr fraction in the gas mixture. The total amount of
24 hydrogen generated by dissociation of HBr (i.e., H and H_2) of course follows the drop in the HBr fraction,
25 as there is no other H-source in the gas mixture, but due to the more pronounced overall dissociation in
26 the plasma at high He fractions, this actually results in an increase of the H atom density. Results are
27 shown for a maximum He fraction of 80%. Of course, applying even higher He fractions up to 100% will
28 eventually decrease the H density towards zero.

1 The HBr^+ ion density closely follows the trend of the HBr density, which is logical, as it is mainly created
2 by electron impact ionization of HBr. It is interesting to see that the Br^+ density increases with He gas
3 fraction, for the same reason as explained above, i.e., the plasma becomes more atomic in nature,
4 allowing for more ionizations and dissociations. Furthermore, the charge transfer from He^+ to Br^+ is
5 another important reason for the higher Br^+ density upon rising He fraction, even up to 80% He. Again,
6 the Br^+ density will rapidly decrease towards zero at 100% He, since there will be no HBr precursor gas
7 present in the plasma. Note that the fluxes of these plasma species towards the wafer (not shown) follow
8 the same trend upon increasing He fraction as the species densities. They determine the etch rates, as will
9 be elaborated in the next section.

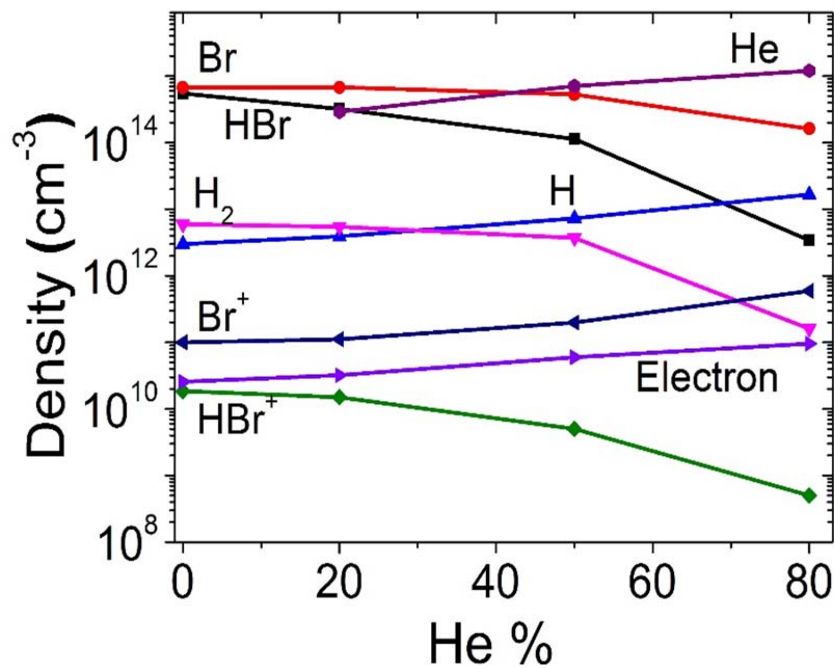

10

11 **Figure 5.** Densities of the most important neutrals and ions as a function of He fraction in the HBr/He mixture. The other
12 operating conditions are the same as in figure 3.

1

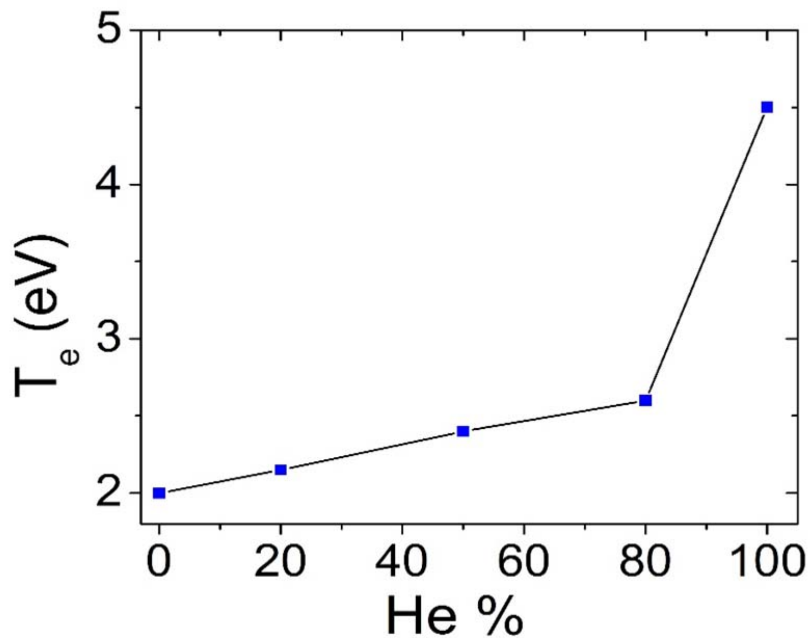

2 **Figure 6.** Electron temperature as a function of He fraction in the HBr/He mixture. The other operating conditions are the same
3 as in figure 3.

4 **Figure 7** shows the chemical composition of the wafer surface during plasma treatment. The H fraction in
5 the surface is about twice as high as the Br fraction, although it was clear from **figure 3** above that the
6 density (and thus flux) of Br is more than one order of magnitude higher than the H density (and flux).
7 The reason for this is that H is more eager to react with Si compared to Br (see **table 4**), and this also
8 explain the lower H density in the plasma. The higher reactivity of H vs Br results in a faster
9 hydrogenation compared to bromination of the surface, even if Br may abstract an H atom from the
10 surface (see **table 4**). Further, the chemical composition is quite uniform along the wafer surface, except
11 for a small increase in H fraction and a decrease in Br fraction at the edge of the wafer (**figure 7a**). The
12 overall chemical composition of the wafer surface as a function of He gas fraction (**figure 7b**), indicates a
13 slight increase in H fraction upon increasing % He. This is like expected because the density of H
14 increases while the Br density decreases upon increasing % He (see **figure 5**) and hence we see a slightly
15 stronger hydrogenation and less bromination effect with increasing He % in the HBr/He mixture.

1

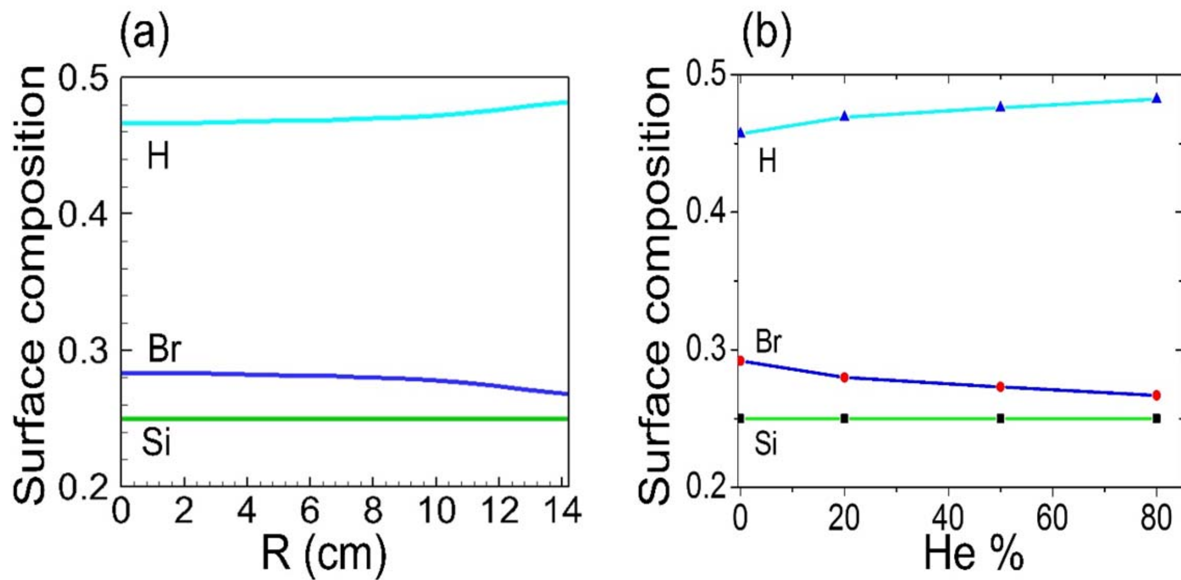

2 **Figure 7.** Chemical composition of the surface, as a function of position on the wafer, for 20% He in the gas mixture (a), and
3 averaged over the wafer surface as a function of He fraction in the HBr/He mixture (b). The other operating conditions are the
4 same as in figure 3.

5 *3.3. Comparison of calculated and experimental etch rates*

6 **Figure 8** shows the calculated and experimental etch rates for different HBr/He mixtures, as a function of
7 position from the centre to the edge of the wafer. The experimental etch rates were obtained by measuring
8 the thickness of the wafer before and after the etch experiment with ellipsometry. The actual etching
9 process was carried out in a Lam Research 2300 Versys Kiyo TCP reactor.The calculated etch rates are
10 more or less in the same range as the experimental values, but the experimental etch rates are less
11 uniform. The experimental data show a maximum etch rate in the center of the wafer at high HBr fraction,
12 changing to a maximum at the edge of the wafer at high He fraction (apart from the 100% He case where
13 the etch rate is ~0 nm/min). This can be explained as follows: At high HBr fractions, chemical etching is
14 very important, and thus dependent on the densities of the reactive neutral species. The HBr gas has a
15 maximum density in the center of the reactor (see also **figure 3** above), because of the inlet which is at the
16 center of the reactor. This will cause a maximum gas flow towards the wafer in the center, producing the
17 reactive species (H and Br), which are responsible for the etching, and this explains the maximum etch
18 rate in the center of the wafer. At high He fraction, chemical etching is less important and physical sputter
19 comes into play, even though the total etch rate becomes much lower. The maximum ion flux towards the
20 wafer is found at a radial position of 6-8 cm, hence corresponding to the position of the coil. This might
21 explain why the maximum etch rate is now not reached at the center but near the edge of the wafer. The
22 calculated etch rates show a much more uniform profile. This might indicate that the effect of the gas
23 flow towards the wafer is underestimated in the model. Indeed, the model predicts maximum densities of
24 the H and Br atoms underneath the coil (see **figure 3** above), which gives rise to maximum fluxes towards
25 the wafer at a radial position of 6-8 cm (see **figure 8**), explaining why the calculated etch rates show a
26 broad maximum at a radial position in this area.

Finally, it is clear from **figure 8** that the Si etch rate drops upon increasing He fraction, from about 120 nm/min in the pure HBr case, to 0 nm/min in the case of pure He. Overall, the etch rate is quite low under these conditions, which is expected when using HBr. Indeed, as mentioned in the introduction, Br is less reactive than Cl and F, which results in a lower etch rate, but it allows for more control during etching and more fine-tuning of the etch rate when fabricating ultra-small features. Even though the ion density is higher at increasing He fraction, the chemical conversion of the wafer surface seems to be the decisive factor that controls the overall etch rate. These results suggest that the introduction of He to a HBr plasma strongly suppresses the formation of SiH_xBr_y ($x \geq 0$, $y \geq 0$, $x+y=4$) etch products, thereby decreasing the etch rate, even when the ion bombardment is higher.

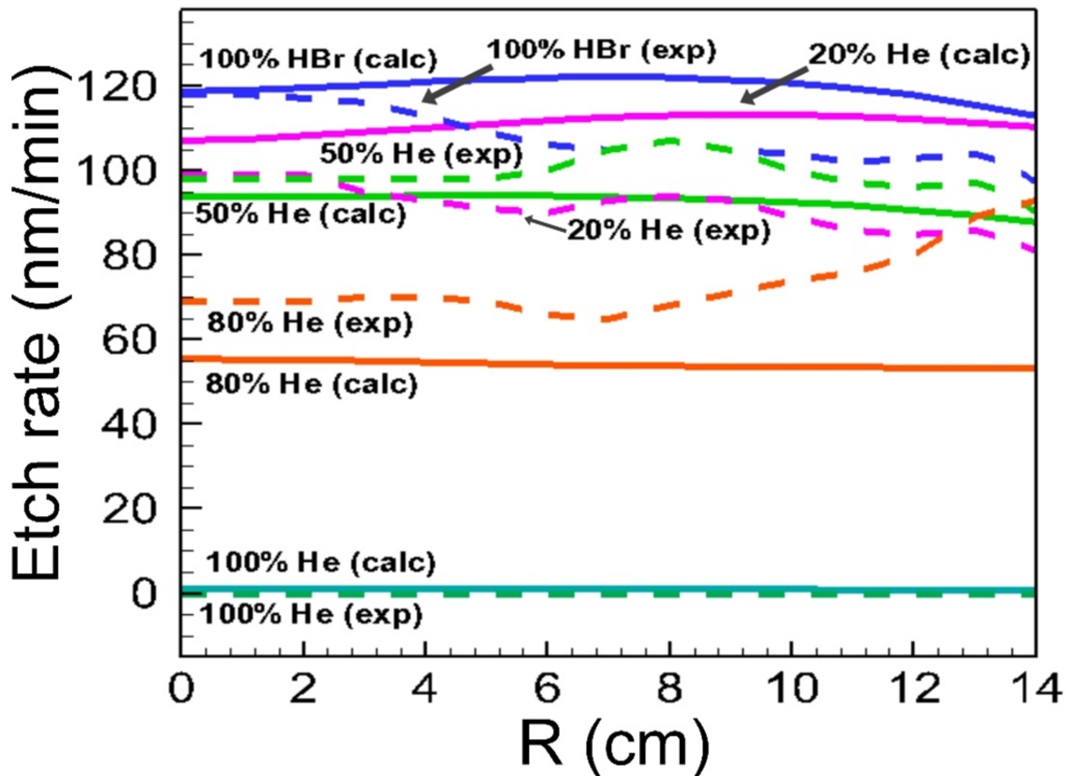

Figure 8. Comparison of experimental and calculated etch rates as a function of position on wafer. The solid lines are the calculated etch rates while the dashed lines represent the experimentally measured etch rates.

Conclusions

We have investigated an inductively coupled plasma in a HBr/He mixture used for the etching of silicon, by means of hybrid Monte Carlo - fluid plasma simulations. Br-containing plasmas are becoming more popular in recent years, due to their lower reactivity towards silicon compared to F and Cl. This allows for fine-tuning of the etch rate for fabrication of ultra-small electronic components. We studied the effect of dilution of the HBr gas with He on the plasma characteristics and on the etch rate of Si, in the range of 0-80 % He in the mixture. When He is added to HBr, the density and flux of Br, which is an important etch species, decreases as expected, and this slows down the formation of chemical etch products (SiH_xBr_y), which in turn leads to an overall decrease in the etch rate. It was also found that the density of the H

1 atoms actually increases with He gas fraction, at least in the range of 0-80% He. The reason is that larger
2 He fractions in the mixture yield a higher electron temperature, because the electrons do not lose their
3 energy so much by vibrational and rotational excitation. Hence, the electron energy can be more
4 efficiently used for ionization and dissociation, resulting in a larger fraction of HBr to become
5 dissociated.

6 For the same reason, the higher He fraction results in a higher total ion density and more pronounced
7 sputtering of the Si surface. However, our results clearly show that the etch rate decreases with He gas
8 fraction, suggesting that chemical etching is still the most important factor determining the overall etch
9 rate. Thus, chemical etching versus physical sputtering can be controlled with the HBr/He mixing ratio.

10 **Acknowledgements**

11 The authors would like to thank the Higher Education Commission of Pakistan (HEC) for financial
12 support under the Indigenous Ph.D. Program Batch-IV and IRSIP (International Research Support
13 Initiative Program). This work was carried out in part using the Turing HPC infrastructure at the CalcUA
14 core facility of the Universiteit Antwerpen, a division of the Flemish Supercomputer Center VSC, funded
15 by the Hercules Foundation, the Flemish Government (department EWI) and the University of Antwerp.

16 **References**

17 [1] Flamm D L 1990 *Pure & Appl. Chem.* ***62*** 1709-1720.
18 [2] Aldao C M and Weaver J H 2001 *Prog. Surf. Sc.* ***68*** 189-230.
19 [3] Winters H F and Coburn J W 1992, *Surf. Sci. Reports.* ***14*** 161-269.
20 [4] Flamm D L, Donnelly V M, Mucha J A 1981 *J. Appl. Phys.* ***52*** 3633-3639.
21 [5] Cardinaud C, Peignon M C, and Tessier P Y 2000 *Applied Surface Science.* ***164*** 72-83.
22 [6] Ogryzlo E A, Ibbotson D E, Flamm D L, and Mucha J A 1990 *J. Appl. Phys.* ***67*** 3115-3120.
23 [7] Oostra D J, Van Ingen R P, Haring A, De Vries A E, and Van Veen G N A 1987 *Appl. Phys. Lett.* ***50*** 1506-1508.
24 [8] Layadi N, Colonell J, and Lee J 1999 *Bell Labs Tech. J.* 155-171.
25 [9] Mahorowala A P, Sawin H H, Jones R and Labun A H 2002 *J. Vac. Sci. Technol.* ***B20(3)*** 1055-1063.
26 [10] Desvoivres L, Vallier L, and Joubert O 2000 *J. Vac. Sci. Technol.* ***B18 (1)*** 156-165.
27 [11] Cheng C and Guinn K 1995 *J. Vac. Sci. Technol,* ***A13 (4)*** 1970-1976.
28 [12] ElMasry A M, Fong F, Wolfe J C and Randall J N 1988 *J. Vac. Sci. Technol.* ***B 6(1)*** 257-262.
29 [13] Cheng C C, Guinn K V, Donelly V M 1996 *J. Vac. Sci. Technol.* ***B 14(1)*** 85-90.
30 [14] Ham Y H, Efremov A, Yun S J , Kim J K , Min N K, and Kwon K H 2009 *Thin Solid Films,* ***517(14)*** 4242-4245.
31 [15] Smirnov A A, Efremov A M, and Svettsov V I 2010 *Russ. Microelectron.* ***39(6)*** 418-426.
32 [16] Ham Y H, Efremov A, Lee H W, Yun S J, Min N K, Baek K H, Do L M, and Kwon K H 2011 *Vacuum,* ***85*** 1021-1025.
33 [17] Lee H W, Kim M, Min N K, Efremov A, Lee C W, and Kwon K H 2008 *Jpn. J. Appl. Phys.* ***47(8)*** 6917-6922.
34 [18] Efremov A, Kim Y, Lee H, and Kwon K 2011 *Plasma Chem Plasma Process.* ***31*** 259-271.
35 [19] Vicknesh S, Ramam A 2004 *J. Electrochem. Soc.* ***151*** C772-C780.
36 [20] Takazava H, Takatani S, Yamamoto S 1996 Jpn. J. Appl. Phys. ***35*** L754-L756.
37 [21] Gomez S, Belen R J, Kiehlbauch M, Aydila E S 2005 *J. Vac. Sci. Technol.* ***A 23*** 1592-1597.
38 [22] Pargon E , Joubert O , Chevolleau T, Cunge G, Xu S, Lill T 2005 J. Vac. Sci. Technol. ***B 23*** 103.
39 [23] Kuo Y, Tai T L 1998 *J. Electrochem. Soc.* ***145*** 4313-4317.
40 [24] Kushner M J *J. Phys. D. Appl. Phys.* ***42*** 194013 1-20.
41 [25] Rauf S and Kushner M 1999 *J. Appl. Phys.* ***85*** 3460-3469.
42 [26] Corrigan S J B 1965 *J. Chem. Phys.* ***43*** 4381-4386.
43 [27] Hayashi M 1979 J. Phys. (Paris) **40** 45-46.
44 [28] Chan C F, ‘‘Reaction cross-sections and rate coefficients related to the production of positive ions’’, *Lawrence Berkeley*
45 *Lab. 1983, Report No. LBID*-632.
46 [29] Banks P, Planet 1966. Sp. Sci. **14** 1085-1103.
47 [30] Kushner M J 1988 *J. Appl. Phys.* ***63*** 2532-2551.
48 [31] Bogaerts A and Gijbels R 2002 *Spectrochim. Acta Part B At. Spectrosc.* ***57(6)*** 1071-1099.
49 [32] Hoekstra R H, Grapperhaus M J, Kushner M J 1997 *J. Vac. Sci. Technol.* ***A 15*** 1913-1921.
50 [33] Tinck S, Bogaerts A 2012, Plasma Porcess. Polym. **9** 522-539
51 [34] Ree J, Chang K S, Moon K H, and Kim Y H *Bull.Korean Chem. Soc.* ***22(8)*** 889-896.

1[35] Kratzera M, Steinhögla W, Kerscha A, Sachsea T and Höinka V 2001 *Mat. Res. Soc.Symp. Proc.* ***677*** AA5.6
2[36] Vitale S A, Chae H, and Sawin H H 2001 *J. Vac. Sci. Technol.* ***A 19(5)*** 2197-2206.
3[37] Matsunami N,Yamamura Y, and Itikawa Y 1984 *atomic data and nuclear data tables.* ***31*** l-80.